JOURNAL OF VIROLOGY, Aug. 1995, p. 4963–4971 Vol. 69, No. 8
0022-538X/95/$04.00+0

Characterization of a Murine Coronavirus Defective Interfering RNA Internal *cis*-Acting Replication Signal

YOUNG-NAM KIM AND SHINJI MAKINO*

Department of Microbiology, The University of Texas at Austin, Austin, Texas 78712-1095

Received 23 December 1994/Accepted 2 May 1995

The mouse hepatitis virus (MHV) sequences required for replication of the JHM strain of MHV defective interfering (DI) RNA consist of three discontinuous genomic regions: about 0.47 kb from both terminal sequences and a 0.13-kb internal region present at about 0.9 kb from the 5 end of the DI genome. In this study, we investigated the role of the internal 0.13-kb region in MHV RNA replication. Overall sequences of the 0.13-kb regions from various MHV strains were similar to each other, with nucleotide substitutions in some strains; MHV-A59 was exceptional, with three nucleotide deletions. Computer-based secondary-structure analysis of the 0.13-kb region in the positive strand revealed that most of the MHV strains formed the same or a similar main stem-loop structure, whereas only MHV-A59 formed a smaller main stem-loop structure. The RNA secondary structures in the negative strands were much less uniform among the MHV strains. A series of DI RNAs that contained MHV-JHM-derived 5 - and 3 -terminal sequences plus internal 0.13-kb regions derived from various MHV strains were constructed. Most of these DI RNAs replicated in MHV-infected cells, except that MRP-A59, with a 0.13-kb region derived from MHV-A59, failed to replicate. Interestingly, replication of MRP-A59 was temperature dependent; it occurred at 39.5 C but not at 37 or 35 C, whereas a DI RNA with an MHV-JHM-derived 0.13-kb region replicated at all three temperatures. At 37 C, synthesis of MRP-A59 negative-strand RNA was detected in MHV-infected and MRP-A59 RNA-transfected cells. Another DI RNA with the internal 0.13-kb region deleted also synthesized negative-strand RNA in MHV-infected cells. MRP-A59-transfected cells were shifted from 39.5 to 37 C at 5.5 h postinfection, a time when most MHV negative-strand RNAs have already accumulated; after the shift, MRP-A59 positive-strand RNA synthesis ceased. The minimum sequence required for maintenance of the positive-strand major stem-loop structure and biological function of the MHV-JHM 0.13-kb region was about 57 nucleotides. Function was lost in the 50-nucleotide sequence that formed a positive-strand stem-loop structure identical to that of MHV-A59. These studies suggested that the RNA structure made by the internal sequence was important for positive-strand MHV RNA synthesis.

Mouse hepatitis virus (MHV), a coronavirus, is an enveloped virus with a single-stranded, positive-sense RNA genome of approximately 31 kb (16, 18, 32). In MHV-infected cells, genomic-size virus-specific mRNA and six or seven species of virus-specific subgenomic mRNAs with a 3′-coterminal nested-set structure (14, 19) are synthesized; these are numbered 1 to 7, in decreasing order of size (14, 19). None of the mRNAs are packaged into MHV virions, except for mRNA 1, which is efficiently packaged because of the presence of a packaging signal (5). The 5′ ends of MHV genomic RNA and subgenomic mRNAs contain a 72- to 77-nucleotide (nt) leader sequence (13, 15, 36).

We have been studying MHV sequences which are necessary for MHV RNA replication by using defective interfering (DI) RNA of MHV. Among different DI RNA species of the JHM strain of MHV (MHV-JHM) (22, 26), we characterized a 2.2-kb DI RNA, DIssE, which is the smallest naturally occurring coronavirus DI RNA (25). This DI RNA consists of three noncontiguous genomic regions; the first region (domain I) represents 0.86 kb from the 5′ end of the genomic RNA; the second region (domain II), 0.75 kb, corresponds to the region 3.1 to 3.9 kb from the 5′ end of genomic RNA; and the third domain (domain III) represents 0.6 kb from the 3′ end of the parental MHV-JHM genome (Fig. 1). Three discontinuous sequences generated from the three domains are required for DIssE replication (11); they include approximately 470 nt at the 5′ terminus, about 460 nt at the 3′ terminus, and 134 nt in an internal position approximately 0.9 kb from the 5′ end of the DI RNA (0.13-kb region). This internal *cis*-acting replication signal mapped at the 5′-most end of the domain II (Fig. 1). Deletion analysis of another MHV-JHM DI RNA, the 3.6-kb DIssF, revealed that the same internal *cis*-acting replication signal is required for DIssF-derived DI RNA replication (20).

Generally, DI RNAs of RNA viruses contain at least one terminal sequence from their helper virus (8). This suggests that viral termini possess a signal(s) which is recognized by viral RNA polymerase. Not surprisingly, the MHV *cis*-acting RNA replication signal includes both MHV termini. More interestingly, an internal sequence is required for MHV-JHM DI RNA replication. In the present study, we have characterized the role of the internal *cis*-acting replication signal in MHV DI RNA replication. Our study indicated that the RNA structure made by the internal *cis*-acting replication signal was important for positive-strand RNA synthesis. We also mapped the biological function of the internal *cis*-acting region to within 57 nt.

* Corresponding author. Mailing address: Department of Microbiology, The University of Texas at Austin, ESB 304, 24th at Speedway, Austin, TX 78712-1095. Phone: (512) 471-6876. Fax: (512) 471-7088. Electronic mail address: makino@mail.utexas.edu.

MATERIALS AND METHODS

Viruses and cells. Plaque-cloned MHV-A59 (14) was used as a helper virus. The MHV strains MHV-1, MHV-2, MHV-S, MHV-NuU, and MHV-3 and its

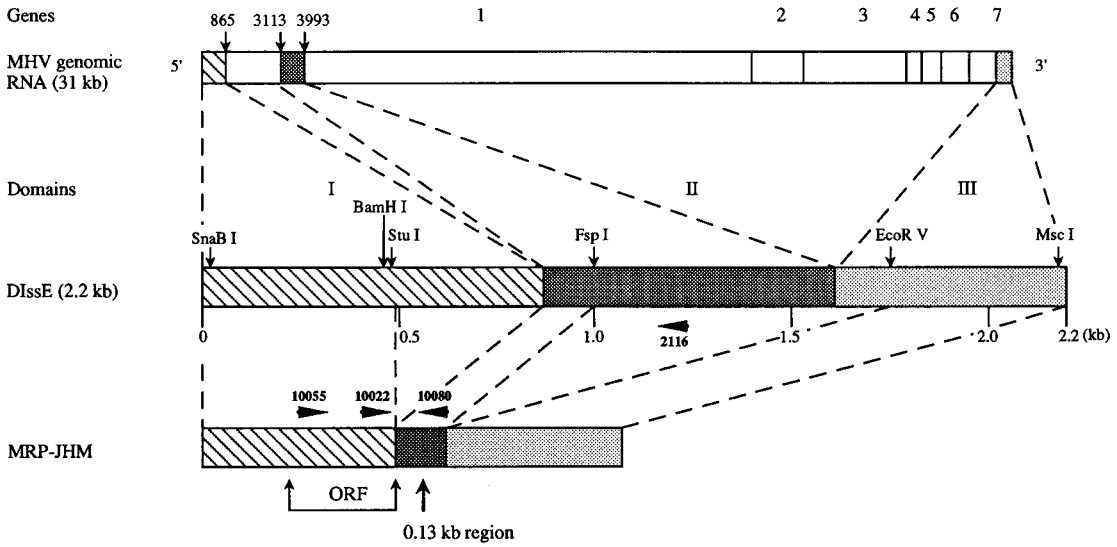

FIG. 1. Diagram of the structure of MRP-JHM compared with those of MHV-JHM genomic RNA and DIssE RNA. Genes 1 through 7 represent the seven genes of MHV. The three domains of DIssE RNA (domains I through III) and the restriction enzyme sites are indicated above the diagram of DIssE. ORF represents the location of the MRP-JHM-specific ORF. Oligonucleotides used for RT-PCR and their binding sites are indicated by arrows. The 0.13-kb region of MRP-JHM represents the internal *cis*-acting signal.

variant MHV-3Yac (17) were obtained from Michael Lai, University of Southern California. Mouse DBT cells (7) were used for growth of viruses.

Preparation of virus-specific intracellular RNA and agarose gel electrophoresis. Virus-specific RNAs in virus-infected cells were prepared as described previously (27). For the study of negative-strand RNA, RNA was extracted with RNAzol B (Cinnex/Biotex Lab) by the procedure suggested by the manufacturer. Virus-specific RNA was labeled with $^{32}P_i$ as previously described (27) and separated by electrophoresis on 1% agarose gels after denaturation with 1 M glyoxal (29).

Plasmid construction. MRP-JHM resulted from insertion of the 0.6-kb *Bam*HI MRD (11) fragment into the large *Bam*HI MP51-2 fragment (23). MHV genomic RNA from one of several MHV strains was mixed with oligonucleotide 10042 (5′-GCAACACAAATTTCCG-3′), which hybridizes with MHV genomic RNA 3,178 to 3,193 nt from the 5′ end, and the cDNA was synthesized as previously described (25). Reverse transcriptase (RT)-PCR products were synthesized by incubating the cDNA products with oligonucleotide 10008 (5′-AA GACGATATCGCAGCGGATGTTGTAGATG-3′), which contains an *Eco*RV site and hybridizes with antisense MHV genomic RNA 100 to 129 nt upstream of the oligonucleotide 10042 binding site in PCR buffer (11), and the samples were incubated at 94°C for 30 s, 42°C for 45 s, and 72°C for 100 s for 25 cycles. The RT-PCR products from genomic RNAs of MHV-A59, MHV-1, MHV-2, MHV-3, MHV-3Yac, MHV-S, and MHV-NuU were blunt ended, phosphorylated, digested with *Eco*RV, and inserted into the *Stu*I-*Eco*RV fragment of MP51-2, yielding MRP-A59, MRP-1, MRP-2, MRP-3, MRP-3Yac, MRP-S, and MRP-NuU, respectively. MRP-JHM-derived deletion mutants were constructed by a PCR-based procedure. The combination of oligonucleotides and the resulting mutants are listed (name of mutant, oligonucleotide binding to negative-sense template, oligonucleotide binding to positive-sense template, template DNA for PCR, insertion site of PCR product) as follows: MRP-JHMΔ1, oligonucleotide 2167 (5′-TATGACTCGGCCGCAACAGATGTTGT-3′), oligonucleotide 2292 (5′-ACAAATTCGCGAATCAGC-3′), MP51-2, MP51-2 *Eco*RV-*Stu*I site; MRP-JHMΔ3, oligonucleotide 2293 (5′-GCAACAGATATCGTAT AT-3′), oligonucleotide 2292, MP51-2, MP51-2 *Eco*RV-*Stu*I site; MRP-JHMΔ4, oligonucleotide 10002 (5′-AACCAAGATATCGATGCT-3′), oligonucleotide 130 (5′-TTCCAATTGGCCATGATCAA-3′), MRP-JHMΔ3, MP51-2 *Eco*RV-*Msc*I; MRP-JHMΔ5, oligonucleotide 95 (5′-GATTGGCGTCCGTACGTA-3′), oligonucleotide 1111 (5′-GAGCCAGAAGGCTGCGAT-3′), MRP-JHMΔ3, MP51-2 *Sna*BI-*Eco*RV site; MRP-JHMΔ6, oligonucleotide 95, oligonucleotide 1111, MRP-JHMΔ4, MP51-2 *Sna*BI-*Eco*RV site; MRP-JHMΔ7, oligonucleotide 10052 (5′-ATGCTGACAGGCCTGTAG-3′), oligonucleotide 130, MRP-JH MΔ6, DE5-w4 (24) *Stu*I-*Msc*I; MRP-JHMΔ8, oligonucleotide 10053 (5′-CCTGT AGGCCTTGTCGCC-3′), oligonucleotide 130, MRP-JHMΔ6, DE5-w4 *Stu*I-*Msc*I. For each mutant, the entire region obtained by insertion of the PCR product was sequenced.

RNA transcription and transfection. Plasmid DNAs were linearized by *Xba*I digestion, except for MRP-JHM, which was linearized by *Eco*RI digestion, and RNA was synthesized in vitro with T7 RNA polymerase as previously described (24). The lipofection method was used for RNA transfection as previously described (23).

RT-PCR analysis of negative-strand RNA. For the analysis of negative-strand RNA, extracted total intracellular RNA samples were incubated with DNase (0.5 U/ml) in a DNase buffer consisting of 100 mM NaCl, 10 mM Tris-hydrochloride (pH 7.8), 2 mM $CaCl_2$, and 2 mM $MgCl_2$ for 20 min at 37°C. Intracellular RNAs were then extracted with phenol-chloroform and precipitated with ethanol. After ethanol precipitation, the RNAs were heat denatured and quickly chilled on ice. For the amplification of negative-strand RNA of MRP-JHMΔ7 and MRP-A59, specific cDNA was synthesized from intracellular RNA as previously described (25), using as a primer oligonucleotide 10055 (5′-TTCCGAACGCATCG GAGAAGTTGGGTAACCCTGAGA-3′) (Fig. 1), which binds to negative-strand MRP-A59 at nucleotides 272 to 307 from the 3′ end; then RT was inactivated by heating the sample to 94°C for 10 min. MHV-specific cDNA was then incubated with oligonucleotide 10080 (5′-GGCAACGCCGTCCTCTTCT TGGGTATCGGC-3′) (Fig. 1), which binds to positive-sense RNA at nt 545 to 574 from the 5′ end of MRP-A59, in PCR buffer at 94°C for 30 s, 55°C for 30 s, and 72°C for 100 s for 20 cycles. For the amplification of MR9 negative-strand RNA, similar experimental conditions were used, except that oligonucleotide 10022 (5′-GTCCGCCATAATCCGT-3′) (Fig. 1), which hybridizes with negative-strand MR9 RNA at nt 429 to 444 from the 3′ end, and oligonucleotide 2116 (5′-ACTTAAGATACTGTCTTC-3′) (Fig. 1), which hybridizes with positive-strand MR9 RNA at nt 802 to 819 from the 5′ end, were used in the place of oligonucleotides 10055 and 10080, respectively. After the amplification, RT-PCR products were examined by Southern blot analysis in which the samples were separated by 1% agarose gel electrophoresis. A gel-purified 0.2-kb *Bst*EII-*Stu*I fragment corresponding to 0.3 to 0.5 kb from the 5′ end of MRP-A59 was used as a probe for the detection of MRP-A59 negative-strand RNA from transfected cells, and a 0.2-kb *Stu*I-*Eag*I fragment corresponding to 0.5 to 0.7 kb from the 5′ end of MR9 was used as a probe for the detection of MR9 negative-strand RNA. A mixture of the following three RNA samples was used as one of the negative controls: intracellular RNA from MHV-A59-infected DBT cells, intracellular RNA from mock-infected DBT cells that were transfected with MRP-A59 RNA, and in vitro synthesized MRP-A59 RNA that had been equilibrated with the amount of replicating MRP-A59 RNA found in cells transfected with MRP-A59 and infected with MHV-A59 at 37°C. The cells that were used to produce the RNA for this mixed-RNA negative control were all maintained at 37°C. A similar negative control sample was used for the analysis of MR9. In this case, MR9 RNA was used instead of MRP-A59.

Direct sequencing of the PCR product. The RT-PCR products were separated by agarose gel electrophoresis and recovered from the gel slices by using GeneClean II (Bio 101, La Jolla, Calif.). Direct PCR sequencing was performed as previously described (10, 38).

RESULTS

Analyses of the 0.13-kb region of various MHV strains. We analyzed the role of the 0.13-kb region in MHV DI RNA replication by first determining whether that region derived

FIG. 2. Nucleotide sequence comparison of the 0.13-kb region of MHV-JHM, MHV-A59, MHV-1, MHV-2, MHV-3, MHV-3Yac, MHV-S, and MHV-NuU. Oligonucleotides 10008 and 10042, used for the plasmid construction, are shown by arrows. Sequences which were identical to MHV-JHM are shown by dashed lines. The three nucleotides which were missing in MHV-A59 RNA are marked by asterisks.

from other MHV strains functioned in DI RNA replication. Cloned RT-PCR products, each of which corresponded to the 0.13-kb region of MHV-JHM, were obtained from genomic RNAs of MHV-A59, MHV-1, MHV-2, MHV-3, MHV-3Yac, MHV-S, and MHV-NuU. Among the MHV 0.13-kb regions, sequence analysis revealed some nucleotide substitutions and an overall sequence similarity; MHV-A59, the exception, had three nucleotides deleted (Fig. 2).

Because many biological functions of RNA molecules are mediated not only by primary sequences but also by higher RNA structures (31), we compared the secondary structures of these MHV 0.13-kb regions by computer-based modeling (39). Analysis of positive-strand RNAs revealed that most of the MHVs share a similar structure within the main stem-loop (Fig. 3). The major stem-loop of MHV-2 included a large end loop and two bulges and was found in most of the MHVs (but not in MHV-A59 or MHV-1). In MHV-1, a smaller end loop, a short stem, and a bulge replaced the large end loop. The main stem-loop of MHV-A59 contained only the large end loop, two stems, and one bulge; it lacked one bulge and one stem, which were found in the major stem-loop of MHV-2. The secondary structure of the negative-strand RNAs was less uniform; MHV-S, MHV-NuU, and MHV-2 formed the same large stem-loop structure, and MHV-JHM and MHV-3Yac produced a similar but much shorter stem-loop structure. MHV-A59, MHV-3, and MHV-1 formed secondary structures which differed from each other and from those of the other MHVs.

Any influence that these MHV 0.13-kb regions, derived from various strains, might have on DI RNA replication was explored. We prepared a parental DI clone, MRP-JHM. MRP-JHM was derived from the 5′-end 482 nt and the 3′-end 462 nt of MHV-JHM genomic RNA, as was the middle 0.13-kb region (Fig. 1). Except for an additional 8 nt at the very 3′ end of the 5′-end region (11), the MRP-JHM sequence therefore consisted entirely of MHV-JHM DI RNA *cis*-acting replication signals. We constructed seven other DI cDNAs; these DI cDNAs were structurally similar to MRP-JHM, but each clone contained a 0.13-kb region derived from a different MHV strain. The clones were named according to the origin of the 0.13-kb region; e.g., MRP-A59 contained an MHV-A59-derived 0.13-kb region. Equal amounts of in vitro synthesized DI RNAs were transfected by lipofection into DBT cell monolayers infected with MHV-A59 helper virus 1 h prior to transfection (23). Virus-specific RNAs were labeled with $^{32}P_i$ for 2 h from 4 to 6 h postinfection (p.i.) in the presence of actinomycin D (27) and analyzed by agarose gel electrophoresis. Most of the DI RNAs replicated efficiently; MRP-A59, notably, did not replicate in repeated experiments (Fig. 4). The replication efficiencies of MRP-3Yac and MRP-2 were somewhat lower than those of the other DI RNAs in some experiments (Fig. 4); in other experiments (data not shown), their replication efficiencies were almost the same as those of the other DI RNAs. These data demonstrated that the 0.13-kb region of most of MHVs functioned in DI RNA replication whereas the same region of MHV-A59 did not.

The positive-strand RNA secondary structure of the MHV-A59 0.13-kb region differed significantly from that of the other MHVs (Fig. 3), and only MRP-A59 failed to replicate in MHV-infected cells. Therefore, we hypothesized that the RNA secondary structure directed by the MHV-A59 0.13-kb region differed from that of the other MHVs in the 0.13-kb region and that this difference was responsible for the inability of MRP-A59 to replicate. To test this possibility, we attempted to manipulate the secondary structure of the 0.13-kb region by changing the temperature. This approach was based on our knowledge that some mutant RNA viruses, which have altered sequences in noncoding regions, show temperature-sensitive phenotypes for RNA synthesis (9). Most probably, in these mutant viruses, an RNA structure made at the nonpermissive

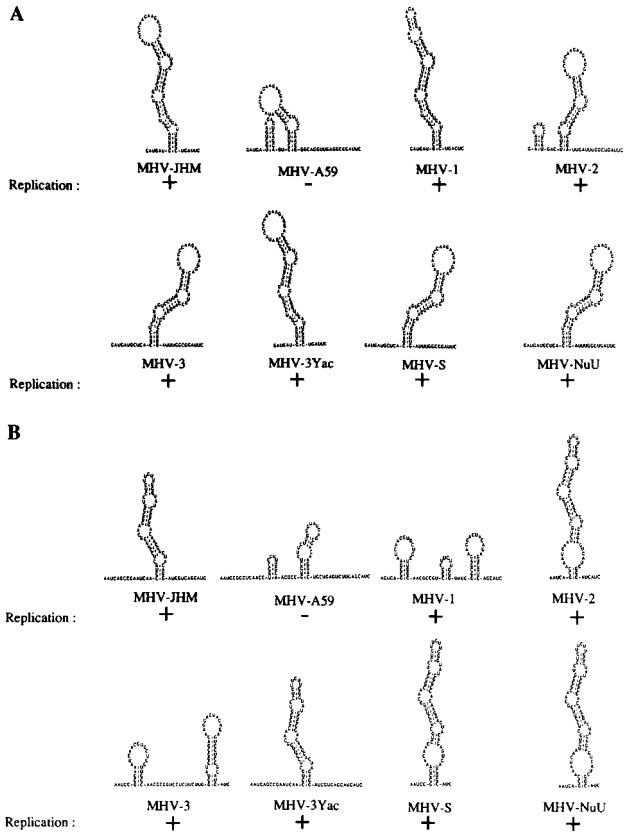

FIG. 3. Predicted secondary structures of the 0.13-kb regions of MHV-JHM, MHV-A59, MHV-1, MHV-2, MHV-3, MHV-3Yac, MHV-S, and MHV-NuU RNA. The secondary structures made by positive-strand RNA (A) and negative-strand RNA (B) are illustrated. The 5′ and 3′ sequences not involved in any specific secondary structure are omitted. The DI RNA with an MHV-A59-derived 0.13-kb region failed to replicate (indicated by −), while DI RNAs which contained other MHV-derived 0.13-kb regions replicated in MHV-A59-infected cells (indicated by +).

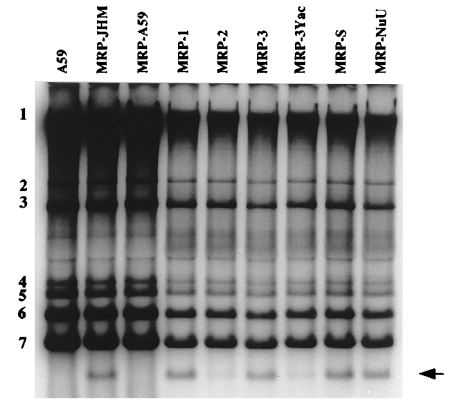

FIG. 4. Replication of MRP-JHM, MRP-A59, MRP-1, MRP-2, MRP-3, MRP-3Yac, MRP-S, and MRP-NuU in DI RNA-transfected, MHV-A59-infected cells. Equal amounts of in vitro synthesized DI RNA were transfected into DBT cell monolayers that had been infected with MHV-A59 helper virus 1 h previously. Virus-specific RNA species were labeled with $^{32}P_i$ from 4 to 6 h p.i. in the presence of actinomycin D, and the extracted RNA was denatured with glyoxal and electrophoresed on a 1% agarose gel. Numbers 1 to 7 represent MHV-specific mRNA species. DI RNAs are indicated by the arrow.

temperature is biologically nonfunctional, whereas at the permissive temperature, regardless of the mutation, mutant virus RNA forms a functional RNA structure. To determine whether replication of MRP-A59 was temperature dependent, we examined replication of MRP-A59 at three different temperatures. Equal amounts of in vitro synthesized MRP-JHM and MRP-A59 were transfected into MHV-A59-infected DBT cells as described above (23). After transfection, virus-infected cells were incubated at either 35, 37, or 39.5°C. Virus-specific RNAs were labeled with $^{32}P_i$ for 2 h from 4 to 6 h p.i., and extracted intracellular RNAs were analyzed by agarose gel electrophoresis. MRP-JHM efficiently replicated at three different temperatures (Fig. 5A) showing increased efficiency with increased temperature; it replicated consistently somewhat less efficiently at 35°C than at the higher temperatures and replicated most efficiently at 39.5°C. Interestingly, MRP-A59, which did not replicate at 35 or at 37°C, replicated efficiently at 39.5°C (Fig. 5). In some experiments, MRP-A59 replicated more efficiently than MRP-JHM at 39.5°C, whereas replication of MRP-A59 at 37°C was not detectable even after longer exposure (Fig. 5B). The data in Fig. 5B unambiguously show that lack of DI RNA replication at 37°C was specific for MRP-A59 but not for MRP-JHM. Clearly MRP-A59 was cold sensitive for replication. We also found that an MHV-JHM-derived DI RNA deletion mutant, MR1 (11), which contains both of the 5′- and 3′-end *cis*-acting replication signals but lacks the internal *cis*-acting replication signal did not replicate at 35, 37, or 39.5°C (data not shown). These data demonstrated that the 0.13-kb region had biological function beyond just serving as a mere spacer region for MRP-A59 at 39.5°C. We checked for additional spontaneous mutations that might have caused the cold-sensitive phenotype by direct sequencing of the RT-PCR product of the 0.13-kb region that was derived from the MRP-A59

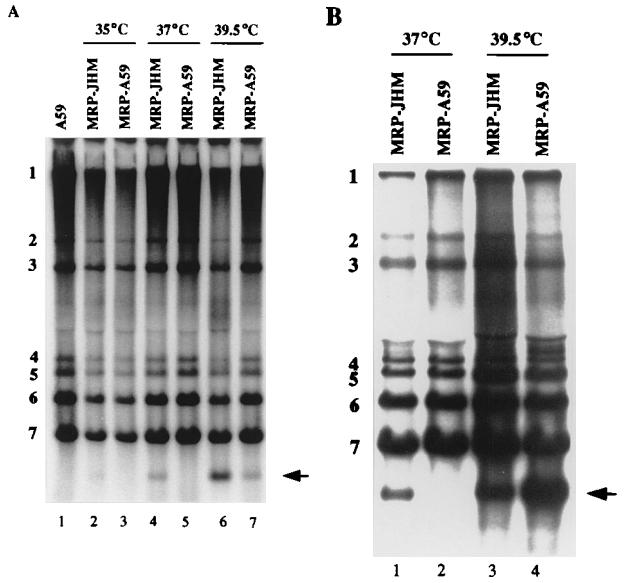

FIG. 5. Cold-sensitive phenotype of MRP-A59 replication. Shown is replication of MRP-JHM and MRP-A59 DI RNAs at different temperatures. Panels A and B represent two independent experiments. Numbers 1 to 7 represent MHV-specific mRNA species. DI RNAs are indicated by arrows. Equal amounts of in vitro synthesized MRP-JHM and MRP-A59 DI RNAs were transfected into DBT cell monolayers infected with MHV-A59 helper virus 1 h prior to transfection and incubated at 35, 37, or 39.5°C. Virus-specific RNA species were labeled with $^{32}P_i$ from 4 to 6 h p.i. in the presence of actinomycin D, and the extracted RNA was denatured with glyoxal and electrophoresed on a 1% agarose gel. MHV-A59-specific RNA extracted from MHV-A59-infected cells cultured at 37°C is shown in panel A, lane 1.

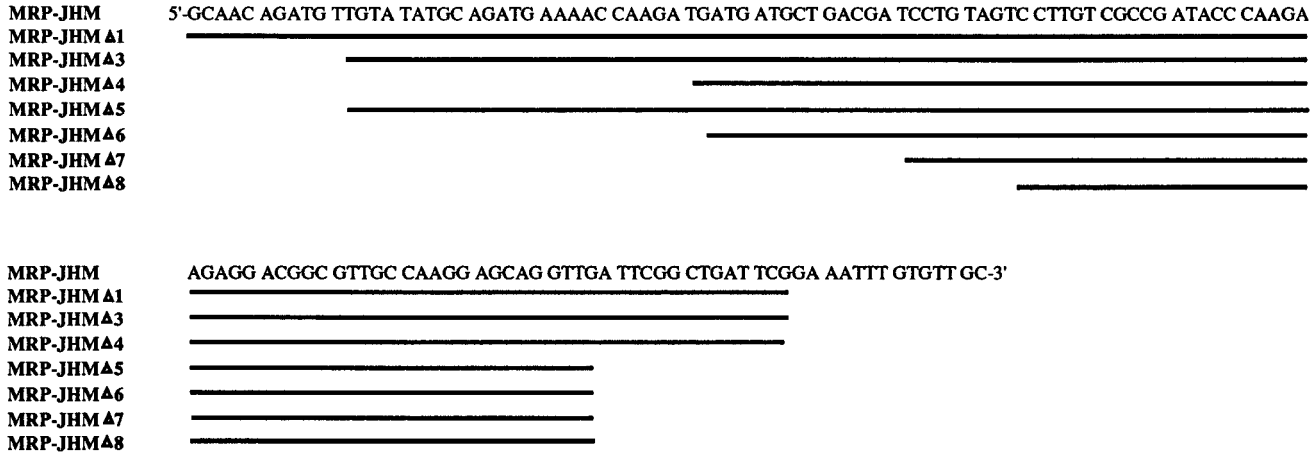

FIG. 6. Nucleotide sequences of the 0.13-kb regions of MRP-JHM and its deletion mutants, MRP-JHMΔ1, MRP-JHMΔ3, MRP-JHMΔ4, MRP-JHMΔ5, MRP-JHMΔ6, MRP-JHMΔ7, and MRP-JHMΔ8. Sequences present in the deletion mutants are indicated by lines.

negative-strand RNA. No sequence change was found. These data strongly suggested that the RNA structures directed by the 0.13-kb region of MRP-A59 at 37 or 35°C did not participate in replication, whereas the structure configured at 39.5°C did function in DI RNA replication. These data supported our speculation that RNA structure mediated the biological function of the 0.13-kb region.

Minimal sequence requirement of the internal *cis*-acting replication signal. As a means of knowing whether the entire 0.13-kb region was required for biological function, we constructed a series of deletion mutants from MRP-JHM and tested them in MHV-A59-infected cells for their ability to replicate. The location of deletion sites is shown in Fig. 6, and their replication is shown in Fig. 7. Most of the deletion mutants replicated; the smallest of these, MRP-JHMΔ7, had an internal sequence of only 57 nt. MRP-JHMΔ8, which lacked an additional 7 nt from the 5′ end of the MRP-JHMΔ7 internal sequence, failed to replicate in repeated experiments. For confirmation of maintenance of the 57-nt sequence in MRP-JHMΔ7 DI RNA-transfected cells, we prepared an RT-PCR product which was specifically amplified from the negative-strand RNA of MRP-JHMΔ7. Direct sequencing analysis of the RT-PCR product corresponding to the 57-nt region demonstrated no sequence change in the replicating MRP-JHMΔ7, demonstrating that the 57 nt was sufficient for biological function of the internal *cis*-acting replication signal.

We analyzed the secondary structures of MRP-JHM-derived deletion mutants to learn whether the main stem-loop structures of positive and negative strands of the 0.13-kb region were maintained in these mutants. Computer-based modeling demonstrated that the major positive-strand RNA stem-loop was completely maintained in MRP-JHMΔ1, MRP-JHMΔ3, MRP-JHMΔ4, MRP-JHMΔ5, MRP-JHMΔ6 (data not shown), and MRP-JHMΔ7 (Fig. 8), whereas only a part of stem-loop structure was maintained in MRP-JHMΔ8. We want to point out that the stem-loop structure made by MRP-JHMΔ8 and the major stem-loop of MHV-A59 0.13 kb were identical (Fig. 3A and 8). Similarly, the major negative-strand RNA stem-loop was conserved in all of the MRP-JHM deletion mutants with replication ability. MRP-JHMΔ8, which did not replicate, contained only a part of the stem-loop structure. This RNA structural analysis demonstrated that the predicted major stem-loop structures found in the positive- and negative-strand RNAs of the 0.13-kb region were maintained in the replication-competent MRP-JHM deletion mutants.

Requirement of the internal *cis*-acting replication signal for positive-strand RNA synthesis. We examined whether the presence of the 0.13-kb region was required for negative-strand DI RNA synthesis by using MRP-A59 and MR9 (11). MR9 is deleted from nt 706 to 1093 from the 5′ end of a DIssE-derived cDNA clone, MRC (11); the deletion includes the entire 0.13-kb region, and MR9 does not replicate in MHV-A59-infected cells (11). Synthesis of negative-strand RNA from the input positive-sense RNAs of these two DI RNAs was examined by RT-PCR; the cDNA was specifically synthesized from the negative-strand RNAs and amplified. At 37°C, which is the nonpermissive temperature for MRP-A59 replication, we looked for synthesis of negative-strand RNA from these DI RNAs.

In separate transfection experiments, we transfected an equal amount of in vitro synthesized RNAs from MRP-A59 and MR9 into uninfected DBT cells or DBT cells preinfected with MHV-A59 3 h prior to transfection, and then we extracted

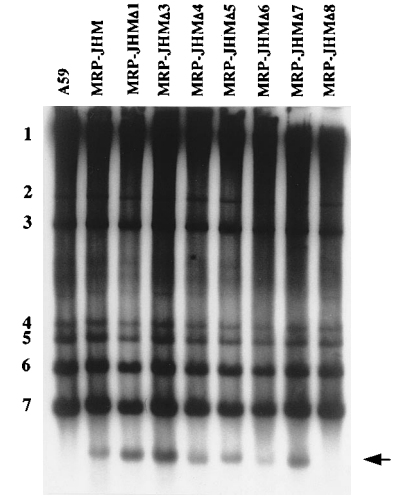

FIG. 7. Replication of MRP-JHM and its deletion mutants. Equal amounts of in vitro synthesized RNAs were transfected into DBT cell monolayers that had been infected with MHV-A59 helper virus 1 h prior to transfection. Virus-specific RNA species were labeled with $^{32}P_i$ from 4 to 6 h p.i. in the presence of actinomycin D, and the extracted RNA was denatured with glyoxal and electrophoresed on a 1% agarose gel. Numbers 1 to 7 represent MHV-specific mRNA species. DI RNAs are indicated by the arrow.

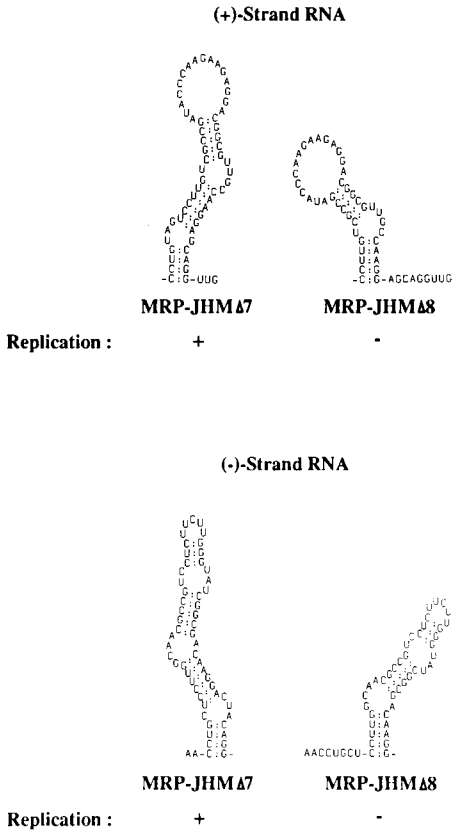

FIG. 8. Predicted secondary structures of internal *cis*-acting replication signals of MRP-JHMΔ7 and MRP-JHMΔ8. Structures of both positive-strand and negative-strand RNAs are shown.

the total intracellular RNA at 8 h posttransfection. We synthesized cDNAs that were both DI specific and negative-strand specific by using oligonucleotide 10055 for MRP-A59 and oligonucleotide 10022 for MR9. After cDNA synthesis, RT was inactivated by heating the sample at 94°C for 10 min. Then, oligonucleotide 10080 was added to the samples from MRP-A59-transfected cells. For RT-PCR of MR9 in the MR9-transfected cells, oligonucleotide 2116 was added. Binding sites of these oligonucleotides to DI RNAs are shown in Fig. 1. After PCR, we checked the RT-PCR products for MRP-A59-specific RT-PCR product and MR9-specific RT-PCR product (Fig. 9); the probes for this Southern blot analysis corresponded to 0.3 to 0.5 kb of MRP-A59 and 0.5 to 0.7 kb of MR9, respectively. In MHV-infected, MRP-A59-transfected cells, we clearly detected DI-specific-0.3 kb RT-PCR products that had been amplified from the negative-strand RNA. This product was not found in the negative controls. Similarly, an expected 0.4-kb RT-PCR product was found in the MR9-transfected, MHV-A59-infected cells, and no signals were found in the negative controls. These data demonstrated that input of plus-sense MRP-A59 and MR9 RNAs yielded negative-strand RNA and that the 0.13-kb region was not necessary for negative-strand RNA synthesis.

Next, we explored the role of the 0.13-kb region in positive-strand RNA synthesis. The in vitro synthesized MRP-A59 RNA was transfected into MHV-A59-infected DBT cells at 3 h p.i. and cultured at 39.5°C, the permissive temperature for MRP-A59 replication. At 5.5 h p.i., the incubation temperature was shifted to the nonpermissive temperature for MRP-A59 replication, 37°C, and MRP-A59 RNA synthesis was examined by $^{32}P_i$ labeling in the presence of actinomycin D for 30 min from 6.5 to 7.0 h p.i. As shown in Fig. 10, we did not detect RNA synthesis of MRP-A59 after the temperature shift, whereas we did detect efficient MRP-A59 replication in the culture that was continuously incubated at 39.5°C. This experiment demonstrated that MRP-A59 RNA synthesis was significantly inhibited after the temperature shift. In cells continuously cultured at 39.5°C, most of the radiolabeled MRP-A59 RNA was poly(A)$^+$, as detected by oligo(dT) column chromatography (data not shown). This was consistent with the fact that MHV positive-strand RNA is at least 100 times more abundant than MHV negative-strand RNA at 6 to 7 h p.i. (35). The efficiency of MHV negative-strand RNA synthesis increases continuously until 6 h p.i. and then declines slightly (35); as a result, a large amount of MRP-A59 negative-strand RNA should have accumulated prior to the labeling period.

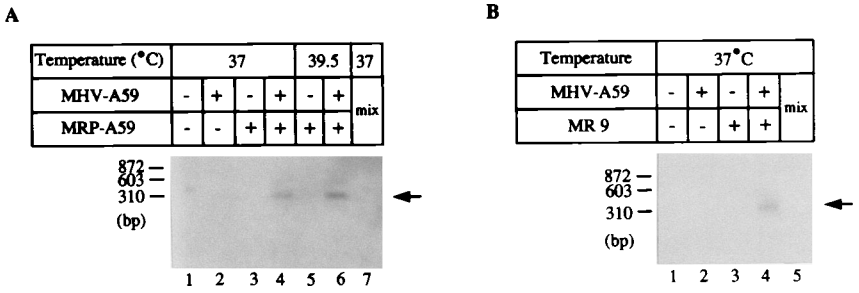

FIG. 9. Southern blot analysis of RT-PCR products synthesized from negative-strand RNAs of MRP-A59 and MR9. The oligonucleotide-binding sites used for RT-PCR are shown in Fig. 1. The DI-specific RT-PCR products are shown by arrows. (A) Analysis of MRP-A59 negative-strand RNA. Equal amounts of in vitro synthesized MRP-A59 RNA were transfected into uninfected DBT cells or DBT cells that had been infected with MHV-A59 3 h prior to transfection, and the cultures were incubated at 37°C (lanes 1 to 4 and 7) or 39.5°C (lanes 5 and 6). Total intracellular RNAs were extracted at 8 h posttransfection. The negative-strand-specific cDNAs were synthesized with oligonucleotide 10055. After cDNA synthesis, RT was inactivated by heating and PCR was performed with oligonucleotides 10055 and 10080. A probe corresponding to 0.3 to 0.5 kb from the 5′ end of MRP-A59 was used for Southern blot analysis. Lanes: 1, mock-infected, mock-transfected cells; 2, MHV-A59-infected, mock-transfected cells; 3 and 5, mock-infected, MRP-A59-transfected cells; 4 and 6, MHV-A59-infected, MRP-A59-transfected cells; 7, a mixture of intracellular RNA from MHV-A59-infected cells, intracellular RNA from MRP-A59-transfected cells, and in vitro synthesized MRP-A59 RNA (see Materials and Methods). (B) Analysis of MR9 negative-strand RNA. Equal amounts of in vitro synthesized MR9 RNA were transfected into uninfected DBT cells or DBT cells infected with MHV-A59 3 h prior to transfection, and cultures were incubated at 37°C. Total intracellular RNAs were extracted at 8 h posttransfection. Oligonucleotide 10022 was used for cDNA synthesis. Oligonucleotides 10022 and 2116 was used for PCR. A probe corresponding to 0.5 to 0.7 kb from the 5′ end of MR9 was used for Southern blot analysis. Lanes 1, mock-infected, mock-transfected cells; 2, MHV-A59-infected, mock-transfected cells; 3, mock-infected, MR9-transfected cells; 4, MHV-A59-infected, MR9-transfected cells; 5, a mixture of intracellular RNA from MHV-A59-infected cells, intracellular RNA from MR9-transfected cells, and in vitro synthesized MR9 RNA (see Materials and Methods).

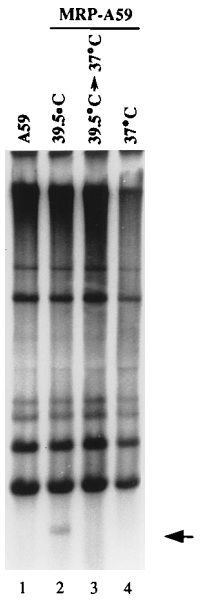

FIG. 10. Effect of temperature shift on MRP-A59 replication. The in vitro synthesized MRP-A59 RNA was transfected into MHV-A59-infected DBT cells at 3 h p.i. and cultured at 39.5°C (lanes 2 and 3) or 37°C (lane 4). At 5.5 h p.i., the incubation temperature was maintained at 39.5°C (lane 2) or at 37°C (lane 4) or shifted to 37°C (lane 3). Virus-specific RNA species were labeled with $^{32}P_i$ from 6.5 to 7 h p.i. in the presence of actinomycin D, and the extracted RNA was denatured with glyoxal and electrophoresed on a 1% agarose gel. MHV-A59-specific RNA extracted from MHV-A59-infected cells cultured at 37°C is shown in lane 1. DI RNA is indicated by the arrow.

The inability to detect radiolabeled MRP-A59 RNA after the temperature shift most probably indicated that positive-strand RNA synthesis did not proceed from the accumulated negative-strand MRP-A59 RNA. The internal *cis*-acting replication signal appeared to drive positive-strand RNA synthesis.

DISCUSSION

The role of the internal *cis*-acting replication signal in MHV DI RNA replication was studied. We demonstrated that the minimum length required for biological function of this region was about 57 nt. Furthermore, our study indicated that the internal *cis*-acting replication signal was responsible for positive-strand RNA synthesis but not for negative-strand RNA synthesis and that the RNA structure made by the 0.13-kb region was critical for its biological function.

We demonstrated that MRP-A59, which included the MHV-A59-derived 0.13-kb region, replicated at 39.5°C but not at 37°C. This observation indicated that the RNA structures made by the MRP-A59 0.13-kb region at the two temperatures differed and that the RNA structure made at 39.5°C but not at 37°C functioned biologically. Helper virus RNA synthesis occurred efficiently at 37°C; because of that, the failure of MRP-A59 replication at 37°C could not have been due to an absence of helper virus-derived *trans*-acting proteins. Also unlikely is that the cold-sensitive phenotype of MRP-A59 was mediated by a DI-specific protein. All naturally occurring MHV DI RNAs so far examined contain a specific large open reading frame (ORF); the size and sequence of the DI-specific ORFs differ among the DI RNA species (25, 37). The role of the large ORF of MHV-JHM-derived DI RNAs in DI RNA replication is not clear, because the large ORF is not necessary for DIssE-derived DI RNA replication (12). All DI RNAs containing the 0.13-kb region had a small DI RNA-specific ORF which terminated at 503 nt from the 5′ end (Fig. 1). This means that these DI RNAs encoded the same DI-specific ORF with the same termination sequence in the 5′ end of the 0.13-kb region. We also found that the 0.13-kb region of MRP-A59 was unchanged at 39.5°C, indicating that the same DI-specific protein was synthesized from the replicating MRP-A59 as was made by other DIs at 37°C. Therefore, it is unlikely that MHV-derived proteins or the DI-specific protein was responsible for the cold-sensitive phenotype of MRP-A59 replication. Rather, it is most likely that the cold-sensitive phenotype resulted from the different RNA structure generated by the MRP-A59 0.13-kb region at 39.5°C.

Analyses of negative-strand RNA synthesis of MRP-A59 and MR9 and the temperature shift experiment with MRP-A59 demonstrated that the 0.13-kb region was required for positive-strand RNA synthesis but not for negative-strand RNA synthesis. These data are consistent with the results of a recent study, which suggest that only the 3′-end sequence of MHV genomic RNA is sufficient for MHV negative-strand RNA synthesis (21). How is the 0.13-kb region involved in positive-strand RNA synthesis? It is possible that the 0.13-kb region interacts with one of the other *cis*-acting replication signals to form a specific RNA structure. Formation of a specific RNA structure may require not only RNA elements but also binding of a virus-specific protein(s) and/or an unidentified cellular protein(s). Binding of a protein to the 0.13-kb region might stabilize the MHV RNA conformation. Formation of a ribonucleoprotein complex with a certain specific RNA structure may be required for positive-strand RNA synthesis. If this hypothesis is correct, coronavirus RNA synthesis may share some similarities with those of bacteriophage Qβ (30). Bacteriophage Qβ replicase interacts with two different internal sites on Qβ RNA (30); this RNA-protein binding appears to affect the Qβ RNA conformation that is needed for initiation of RNA synthesis. Computer-based modeling of the 0.13-kb region suggested that the RNA secondary structure on negative-strand RNA was quite different among MHVs, whereas positive-strand RNA secondary structure was relatively conserved (Fig. 3). MHV-A59 demonstrated the most divergent positive-strand secondary structure. Only MRP-A59, which contained the MHV-A59-derived 0.13-kb region, failed to replicate at 37°C. Furthermore, replication-incompetent MRP-JHMΔ8, with an internal sequence of just 50 nt, formed the same positive-strand major stem-loop structure found in MHV-A59, whereas the replication-competent MRP-JHMΔ7, with a 57-nt internal sequence, formed the same major positive-strand stem-loop structure as did MHV-2. Therefore, it is tempting to speculate that the positive-strand RNA structure of the 0.13-kb region is important for positive-strand RNA synthesis. We do not know whether the RNA secondary structures predicted by the computer-based modeling are the same as those formed by actual RNA molecules. Biochemical examination of RNA secondary structure in solution and site-directed mutagenesis analysis of the 0.13-kb region should verify our speculation. There are several examples in which viral positive-strand RNA secondary structure promotes virus positive-strand RNA synthesis. In poliovirus, a ribonucleoprotein complex that is important for initiation of new positive-strand RNA is proposed to consist of a cellular protein, a virus-specific protein, 3CD, and about 90 nt from the 5′ end of the positive strand (1, 2). Similarly, the structure of the 5′ region of brome mosaic virus positive-strand RNA is important for positive-strand RNA synthesis (33). Another example is the TAR element of human immunodeficiency virus (HIV) (34). The TAR element, which is a stable stem-loop RNA structure present at the 5′ end of HIV mRNAs, forms a ribonucleopro-

tein complex with HIV Tat protein and a cellular protein(s). Formation of the ribonucleoprotein complex is important for efficient transcription of HIV mRNAs (34).

Naturally occurring MHV-A59 DI RNA (DI-a) consists of three noncontiguous regions: the 5′-end 3.9 kb derived from the 5′ end of the genome, an internal sequence of 0.8 kb derived from 20.0 to 20.8 kb from the 5′ end of the genome, and the 3′-end 0.8 kb from the 3′ end of the parental MHV-A59 genomic RNA (37). *cis*-acting RNA replication signals have not yet been described in MHV-A59 DI RNA. As shown in this study, the MHV-A59-derived 0.13-kb region did not support DI RNA replication at 37°C, suggesting noninvolvement of that region in *cis*-acting replication signals of MHV-A59-derived DI RNA that replicates at 37°C. This idea is supported by two other lines of experimentation. A deletion mutant study of an MHV-A59-derived DI RNA showed that this 0.13-kb region is not required for RNA replication (4, 37). Similarly, an MHV-A59-derived synthetic DI RNA, which lacks a region corresponding to the MHV-JHM 0.13-kb region, can replicate in MHV-A59-infected cells (28). This synthetic DI RNA also consists of three different genomic regions: the 5′-end 0.5 kb from the parental MHV-A59, an internal 15 nt from a non-MHV sequence and the 3′-end 1.8 kb from the 3′ end of MHV-A59 (28). The structural and replication capabilities of these MHV-A59 DI RNAs are consistent with our present finding that MRP-A59 containing an MHV-A59-derived 0.13-kb region did not replicate at 37°C.

Do MHV-A59 DI RNAs require only terminal sequences for RNA replication? Recently, we found that a synthetic MHV-A59 RNA made entirely from terminal MHV-A59 genomic sequences (0.5 kb from the 5′ end and 0.5 kb from the 3′ end) failed to replicate in MHV-A59-infected cells, whereas another MHV-A59-derived RNA, including the MHV-JHM 0.13-kb internal sequence inserted between the termini, replicated in MHV-A59-infected cells at 37°C (unpublished data). These data indicated that the presence of only terminal MHV-A59 sequences was not sufficient for MHV-A59 DI RNA replication. We speculate that a region(s) which operates like the 0.13-kb region of MHV-JHM is required for MHV-A59 DI RNA replication too. Our data presented in this paper indicated that the secondary structure of the internal *cis*-acting replication signal was important for RNA synthesis. An MHV-A59 element(s) present in replication-competent MHV-A59 DI RNAs might form an RNA structure similar to the structure formed by the MHV-JHM 0.13-kb region, and such a secondary structure may very well be a requirement for MHV-A59 DI RNA replication. A functionally similar RNA element in MHV-A59 DI RNA may be located quite differently from that of the MHV-JHM 0.13 kb region. The above speculations are likely to be correct, because we recently found that an MHV-JHM genomic region, which mapped outside of the *cis*-acting replication signal, had the same biological function as the 0.13-kb region of MHV-A59 (12a). Parental MHV genomic RNA may contain multiple genomic regions, which have the same biological function as the internal *cis*-acting replication signal of MHV-JHM DI RNA. Some of them may be necessary for efficient MHV genomic RNA replication, whereas MHV DI RNA contains only one or two of these functional regions.

Several other positive-strand RNA viruses each contain their own internal *cis*-acting RNA replication signal (3, 6, 30); however, the function of these signals in viral RNA synthesis is largely unknown. Further analysis of the function of MHV DI RNA internal *cis*-acting replication signals will contribute to the understanding of the coronavirus RNA replication mechanism and should shed light on the replication mechanism of other RNA viruses.

ACKNOWLEDGMENTS

We thank Michael Lai for MHV-1, MHV-2, MHV-S, MHV-NuU, and MHV-3 and its variant MHV-3Yac.

This work was supported by Public Health Service grants AI29984 and AI32591 from the National Institutes of Health.

REFERENCES

1. **Andino, R., G. E. Rieckhof, P. L. Achacoso, and D. Baltimore.** 1993. Poliovirus RNA synthesis utilizes an RNP complex formed around the 5′-end of viral RNA. EMBO J. **12:**3587–3598.
2. **Andino, R., G. E. Rieckhof, and D. Baltimore.** 1990. A functional ribonucleoprotein complex forms around the 5′ end of poliovirus RNA. Cell **63:**369–380.
3. **Ball, L. A., and Y. Li.** 1993. *cis*-acting requirements for the replication of flock house virus RNA 2. J. Virol. **67:**3544–3551.
4. **de Groot, R. J., R. G. van der Most, and W. J. M. Spaan.** 1992. The fitness of defective interfering murine coronavirus DI-a and its derivatives is decreased by nonsense and frameshift mutations. J. Virol. **66:**5898–5905.
5. **Fosmire, J. A., K. Hwang, and S. Makino.** 1992. Identification and characterization of a coronavirus packaging signal. J. Virol. **66:**3522–3530.
6. **Frech, R., and P. Ahlquist.** 1987. Intercistronic as well as terminal sequences are required for efficient amplification of brome mosaic virus. J. Virol. **61:**1457–1465.
7. **Hirano, N., K. Fujiwara, S. Hino, and M. Matsumoto.** 1974. Replication and plaque formation of mouse hepatitis virus (MHV-2) in mouse cell line DBT culture. Arch. Gesamte Virusforsch. **44:**298–302.
8. **Holland, J.** 1991. Defective viral genomes, p. 151–165. *In* B. N. Fields and D. M. Knipe (ed.), Fundamental virology, 2nd ed. Raven Press, New York.
9. **Jacobson, S. J., D. A. Konings, and P. Sarnow.** 1993. Biochemical and genetic evidence for a pseudoknot structure at the 3′ terminus of the poliovirus RNA genome and its role in viral RNA amplification. J. Virol. **67:** 2961–2971.
10. **Joo, M., and S. Makino.** 1992. Mutagenic analysis of the coronavirus intergenic consensus sequence. J. Virol. **66:**6330–6337.
11. **Kim, Y.-N., Y. S. Jeong, and S. Makino.** 1993. Analysis of *cis*-acting sequences essential for coronavirus defective interfering RNA replication. Virology **197:**53–63.
12. **Kim, Y.-N., M. M. C. Lai, and S. Makino.** 1993. Generation and selection of coronavirus defective interfering RNA with large open reading frame by RNA recombination and possible editing. Virology **194:**244–253.

12a. **Kim, Y.-N., and S. Makino.** Unpublished data.

13. **Lai, M. M. C., R. S. Baric, P. R. Brayton, and S. A. Stohlman.** 1984. Characterization of leader RNA sequences on the virion and mRNAs of mouse hepatitis virus, a cytoplasmic RNA virus. Proc. Natl. Acad. Sci. USA **81:**3626–3630.
14. **Lai, M. M. C., P. R. Brayton, R. C. Armen, C. D. Patton, C. Pugh, and S. A. Stohlman.** 1981. Mouse hepatitis virus A59: mRNA structure and genetic localization of the sequence divergence from hepatotropic strain MHV-3. J. Virol. **39:**823–834.
15. **Lai, M. M. C., C. D. Patton, R. S. Baric, and S. A. Stohlman.** 1983. Presence of leader sequences in the mRNA of mouse hepatitis virus. J. Virol. **46:**1027–1033.
16. **Lai, M. M. C., and S. A. Stohlman.** 1978. RNA of mouse hepatitis virus. J. Virol. **26:**236–242.
17. **Lamontagne, L., and J. M. Dupuy.** 1986. Characterization of a non-pathogenic MHV 3 variant derived from a persistently infected lymphoid cell line. Adv. Exp. Med. Biol. **218:**255–263.
18. **Lee, H.-J., C.-K. Shieh, A. E. Gorbalenya, E. V. Eugene, N. La Monica, J. Tuler, A. Bagdzhadzhyan, and M. M. C. Lai.** 1991. The complete sequence (22 kilobases) of murine coronavirus gene 1 encoding the putative proteases and RNA polymerase. Virology **180:**567–582.
19. **Leibowitz, J. L., K. C. Wilhelmsen, and C. W. Bond.** 1981. The virus-specific intracellular RNA species of two murine coronaviruses: MHV-A59 and MHV-JHM. Virology **114:**39–51.
20. **Lin, Y.-J., and M. M. C. Lai.** 1993. Deletion mapping of a mouse hepatitis virus defective interfering RNA reveals the requirement of an internal and discontiguous sequence for replication. J. Virol. **67:**6110–6118.
21. **Lin, Y.-J., C.-L. Liao, and M. M. C. Lai.** 1994. Identification of the *cis*-acting signal for minus-strand RNA synthesis of a murine coronavirus: implications for the role of minus-strand RNA in RNA replication and transcription. J. Virol. **68:**8131–8140.
22. **Makino, S., N. Fujioka, and K. Fujiwara.** 1985. Structure of the intracellular defective viral RNAs of defective interfering particles of mouse hepatitis virus. J. Virol. **54:**329–336.
23. **Makino, S., M. Joo, and J. K. Makino.** 1991. A system for study of coronavirus mRNA synthesis: a regulated, expressed subgenomic defective interfering RNA results from intergenic site insertion. J. Virol. **65:**6031–6041.

24. **Makino, S., and M. M. C. Lai.** 1989. High-frequency leader sequence switching during coronavirus defective interfering RNA replication. J. Virol. **63:** 5285–5292.
25. **Makino, S., C.-K. Shieh, L. H. Soe, S. Baker, and M. M. C. Lai.** 1988. Primary structure and translation of a defective interfering RNA of murine coronavirus. Virology **166:**550–560.
26. **Makino, S., F. Taguchi, and K. Fujiwara.** 1984. Defective interfering particles of mouse hepatitis virus. Virology **133:**9–17.
27. **Makino, S., F. Taguchi, N. Hirano, and K. Fujiwara.** 1984. Analysis of genomic and intracellular viral RNAs of small plaque mutants of mouse hepatitis virus, JHM strain. Virology **139:**138–151.
28. **Masters, P. S., C. A. Koetzner, C. A. Kerr, and Y. Heo.** 1994. Optimization of targeted RNA recombination and mapping of a novel nucleocapsid gene mutation in the coronavirus mouse hepatitis virus. J. Virol. **68:**328–337.
29. **McMaster, G. K., and G. G. Carmichael.** 1977. Analysis of single- and double-stranded nucleic acids on polyacrylamide and agarose gels by using glyoxal and acridine orange. Proc. Natl. Acad. Sci. USA **74:**4835–4838.
30. **Meyer, F., H. Weber, and C. Weissman.** 1981. Interactions of Qβ replicase with Qβ RNA. J. Mol. Biol. **153:**631–660.
31. **Ollis, D. L., and S. W. White.** 1987. Structural basis of protein-nucleic acid interactions. Chem. Rev. **87:**981–995.
32. **Pachuk, C. J., P. J. Bredenbeek, P. W. Zoltick, W. J. M. Spaan, and S. R. Weiss.** 1989. Molecular cloning of the gene encoding the putative polymerase of mouse hepatitis virus, strain A59. Virology **171:**141–148.
33. **Pogue, G. P., and T. C. Hall.** 1992. The requirement for a 5′ stem-loop structure in brome mosaic virus replication supports a new model for viral positive-strand RNA initiation. J. Virol. **66:**674–684.
34. **Rounseville, M., and A. Kumar.** 1992. Binding of a host cell nuclear protein to the stem region of human immunodeficiency virus type 1 *trans*-activation-responsive RNA. J. Virol. **66:**1688–1694.
35. **Sawicki, S. G., and D. L. Sawicki.** 1986. Coronavirus minus-strand RNA synthesis and effect of cycloheximide on coronavirus RNA synthesis. J. Virol. **57:**328–334.
36. **Spaan, W., H. Delius, M. Skinner, J. Armstrong, P. Rottier, S. Smeekens, B. A. M. van der Zeijst, and S. G. Siddell.** 1983. Coronavirus mRNA synthesis involves fusion of non-contiguous sequences. EMBO J. **2:**1939–1944.
37. **van der Most, R. G., P. J. Bredenbeek, and W. J. M. Spaan.** 1991. A domain at the 3′ end of the polymerase gene is essential for encapsidation of coronavirus defective interfering RNAs. J. Virol. **65:**3219–3226.
38. **Winship, P. R.** 1989. An improved method for directly sequencing PCR material using dimethyl sulfoxide. Nucleic Acids Res. **17:**1266.
39. **Zuker, M., and P. Steigler.** 1981. Optimal computer folding of large RNA sequences using thermodynamics and auxiliary information. Nucleic Acids Res. **9:**133–148.